NASA-CR-172287
19840008072

NASA Contractor Report 172287

INTERACTING BOUNDARY-LAYER SOLUTIONS FOR LAMINAR SEPARATED FLOW PAST AIRFOILS

O. R. Burggraf

THE OHIO STATE UNIVERSITY RESEARCH FOUNDATION
Columbus, Ohio 43210

Grant NSG-1622
January 1984

National Aeronautics and
Space Administration

Langley Research Center
Hampton, Virginia 23665

PREFACE

The work described in this report was carried out under Grant No. NSG 1622, "Viscous Interaction Effects on Airfoil Performance." The program was monitored by Dr. Richard Barnwell and Mr. Joel Everhart, Transonic Aerodynamics Division, NASA Langley Research Center. The principle investigator was Dr. Odus R. Burggraf, Department of Aeronautical and Astronautical Engineering, The Ohio State University. Dr. Burggraf's coworkers on the project were, seriatim, Dr. Peter Duck, Dr. C. J. Woan, and Mr. Robert Biedron. This report constitutes the final technical report for the project.

CONTENTS

LIST OF SYMBOLS

A	Matrix coefficient (subdiagonal element); coefficient in discretized Hilbert integral, Appendix A.
B	Matrix coefficient (subdiagonal element).
c	Chord length.
c_F	Skin-friction coefficient.
c_p	Pressure Coefficient.
c_{ij}	Coefficient in discretized interaction condition.
C_L	Lift coefficient.
D	Matrix coefficient (diagonal element).
f	$d\xi/dx$, Appendix B.
F	Normalized stream function.
g	$d\eta/dy$, Appendix B.
h	Grid spacing.
I_h^{2h}, I_{2h}^h	Fine-grid to coarse-grid screening operation, interpolation operator, respectively.
J_1	Value of Hilbert integral, Appendix A.
K	Coefficient in interaction condition, see Eqs. (7) and (9).
$\mathcal{L}_h$	Finite-difference operator with grid spacing h, Appendix B.
M	Number of points in s-grid.
N	Number of points in η-grid; also number of points along wake centerline. (p.21).
N_0	Initial number of points on grid.
NX	Option number for two-point or three-point x-differencing.
P	Matrix coefficient (last column).
r_v	Relaxation factor in interaction condition.

R	Element of right-side column vector of matrix equation.
$R_h^{(1)}, R_h^{(2)}$	Residuals of difference equations on h grid, Appendix B.
R_N	Reynolds number, $u_\infty c/\nu$.
s	x/c, normalized boundary-layer coordinate (surface oriented).
S	Matrix coefficient (superdiagonal element).
u	Velocity component in x-direction.
u_s	Inviscid flow speed at surface.
v	Velocity component in y-direction.
x	Boundary-layer coordinate measured along airfoil surface and wake centerline; potential-flow coordinate parallel to freestream.
x_o	Point of initiation of boundary-layer computation.
x_1	Initial point on airfoil for full interaction.
x_2	Downstream cutoff point for viscous-wake computation.
X	x/c, normalized potential-flow coordinate (parallel to freestream).
y	Boundary-layer coordinate measured normal to airfoil surface or wake centerline; potential-flow coordinate normal to freestream.
α	Angle of attack.
β	Coefficient in boundary-layer momentum equation.
Γ	Circulation.
$\delta; \delta^*$	Boundary-layer thickness scale; displacement thickness.
δF	Change of F in one iteration.
Δ^*	Normalized displacement thickness.
η	y/δ, normalized boundary-layer coordinate perpendicular to surface.
θ	Angle variable in polar coordinates, Appendix B.

ν	Kinematic viscosity coefficient.
ξ	Transformed x-coordinate for potential flow, Appendix B.
ϕ	Dependent variable, Appendix B.
ω	Relaxation factor in potential-flow computation, Appendix B.
∇_h^2	Finite-difference approximation to Laplace operator.

Subscripts

e	External flow conditions at edge of boundary layer.
i	Grid-point index for x-coordinate.
j	Grid-point index for y or η-coordinate; also used for x-coordinate in interaction condition.
N	Conditions at edge of η-grid.
s	Surface value.
TE	Trailing edge.
x,y	Partial derivative, Appendix B.
∞	Freestream conditions.

Supercripts

n	Iteration index.
*	Modified value.
$-$	Dummy variable.
$\hat{}$	Approximation at current stage of solution, Appendix B.
+	Update value in iteration procedure, Appendix B.
$'$	Partial derivative with respect to η.
$\sim$	Deviation from current approximation, Appendix B.

SUMMARY

Numerical solutions of the interacting laminar boundary-layer equations are presented for two symmetric airfoils at zero incidence: the NACA 0012 and the NACA 66_3-018 airfoils. The potential flow was computed using Carlson's code, and viscous interaction was treated following a Hilbert-integral scheme due to Veldman. Effects of various grid parameters are studied, and pressure and skin-friction distributions are compared at several Reynolds numbers. For the NACA 0012 airfoil, Reynolds number is varied from a value just below separation (R_N = 3000) to a value for which extensive separation occurs (R_N = 100,000). For the 66_3-018 airfoil, results are given at intermediate values (R_N = 10,000 and 40,000). The method fails to converge for greater values of Reynolds number, corresponding to the development of very thin well-separated shear layers where transition to turbulence would occur naturally.

INTRODUCTION

A major problem in computational aerodynamics is the prediction of maximum lift coefficient for two-dimensional wing sections. The numerical solution of this problem would involve computation of the flow past airfoils at large angles of attack, including conditions of separation and stall. At large Reynolds number the boundary-layer model is appropriate, provided viscous interaction is included; in fact, separation bubbles of moderate extent have been analyzed on the basis of such a model. The long-term goal of this study is to carry out such computations for airfoils at moderate angles of attack, with the hope that a computation of this type would provide aerodynamic data up to inception of massive separation. However, the present study has been restricted to zero angle of attack, with emphasis on the complications of laminar separation and wake flow that arise with that condition.

The computer program developed for this study is based on the laminar-flow condition. This was desirable for two reasons: (1) leading-edge separation, which can limit the maximum lift, is usually of laminar type, and (2) the basic interaction phenomenon is the same for laminar and turbulent flow, while the equations of motion are simpler in the former case. In addition, laminar flow solutions are of interest for their own sake. For higher Reynolds numbers, an appropriate turbulence model can be incorporated.

Various computer codes are available for the potential-flow portion of the computations. A code developed by Carlson (Ref. 1) for airfoil analysis and design was selected for adaptation to our use; it is well-documented and structured in a way that readily permits interaction with a boundary-layer code in both direct and inverse modes of solution. Since our current interest is in low-speed flow, a simplified version of Carlson's code was programmed for the special case of incompressible flow. In addition, the multigrid technique was incorporated to accelerate convergence of the potential-flow computations. Our implementation of the multigrid procedure, as applied to Carlson's program, is described in Appendix B.

A new boundary-layer code was developed based on a stream-function formulation that permits a natural treatment of interaction. Direct, inverse, and interaction modes all are included in the solution procedure, with switching between modes permitted at any streamwise station. Details of the method are given in the body of this report.

An attempt was made to couple the potential-flow and boundary-layer codes and operate each in the inverse mode. However, a converged solution was not achieved by this method. Instead, an alternative fully interacting scheme was developed successfully. This method and results obtained with it are discussed in the following sections.

INTERACTION THEORY

In the classical boundary-layer theory proposed by Prandtl, the pressure gradient acting on the boundary layer is prescribed by the inviscid (potential flow) solution and the boundary-layer properties, such as the displacement thickness, result from the solution. Prandtl (Ref. 2) also proposed that the pressure distribution could be determined to higher-order accuracy by recalculating the potential flow, accounting for the displacement thickness of the boundary layer. This scheme of accounting for the viscous effect on the potential flow is known as weak-interaction theory. Unfortunately it fails when boundary-layer separation occurs, since Goldstein (Ref. 3) has shown that the boundary-layer solution at separation is singular when the pressure gradient is prescribed, so that an accurate computation must break down at the separation point. Catherall and Mangler (Ref. 4) showed that this difficulty can be overcome by treating the boundary-layer problem as an inverse problem, thus solving for the pressure distribution which would produce a specified displacement thickness. Of course, in practice neither pressure gradient nor displacement thickness are known a priori.

The successful treatment of flow separation as an inverse problem, contrasted with the failure of the classical theory, indicates that separated flows are of the strong-interaction type; i.e., the equations of the external potential flow and of the boundary layer must be coupled and solved simultaneously. A qualitative theory of viscous interaction based on this concept was presented by Crocco and Lees (Ref. 5). The idea also appears in the early work of Lighthill (Ref. 6), and a rational theory has evolved in more recent times in the independent works of Neiland (Ref. 7), Stewartson and Williams (Ref. 8), and Messiter (Ref. 9). This theory, termed the triple-deck by Stewartson, is valid as an asymptotic solution of the laminar Navier-Stokes equations in the limit of infinite Reynolds number. (We note that Prandtl's boundary-layer theory is a valid limit solution for unseparated flows in the same sense.)

The first complete problem to be solved in triple-deck theory was that of the viscous interaction at the trailing edge of a flat plate*. This problem is an example of one for which the classical weak-interaction theory fails. The interaction is caused by the discontinuous change from a no-slip condition on the plate to a no-stress condition on the wake centerline. The resulting solution of the classical boundary-layer theory exhibits a singularity in the slope of the displacement surface for $x = 0^+$ ($x = 0$ at the trailing edge), and a corresponding singularity then is produced in the inviscid pressure distribution if the computation is pursued in the classical manner. In triple-deck theory, the viscous lower-deck solution is determined simultaneously with the inviscid upper deck and no singularity develops. The solution was obtained first by Jobe and Burggraf (Ref. 10), and confirmed by Veldman and Van de Vooren (Ref. 11) and by Chow and Melnik (Ref. 12). A summary of the results is given by Figure 1. The skin friction shown there is normalized by the Blasius (non-interacting) value; the effect of interaction is seen to raise the value by about one third of the Blasius value at the trailing edge. Correspondingly, the pressure on the plate is reduced below the freestream value, and then quickly rises in the wake to a level above the freestream value with a slow decay downstream.

Chow and Melnik (Ref. 12) went on to consider the flat plate at angle of attack. The triple deck then substitutes for the Kutta condition in classical airfoil theory, and in fact the solution gives the viscous correction to the ideal lift of the airfoil. For fixed (but large) Reynolds number, viscous loss of lift is a relatively weak function of angle of attack for small α, but appears to increase catastrophically as α approaches the stall limit. Actually the computation scheme failed before the stall limit was reached, but an estimate was made by extrapo-

*Stewartson and Williams (Ref. 9) solved for the upstream eigenfunctions in supersonic flow, but did not match these to particular downstream disturbances.

lation of the computed results to the point at which separation first occurred at the trailing edge. Thus the first rational prediction of $C_{L_{max}}$ (maximum lift coefficient) was made on the basis of triple-deck theory. Of course for the flat plate in laminar flow, $C_{L_{max}}$ is likely to be determined by leading-edge separation, whereas the analysis of Chow and Melnik is restricted to the vicinity of the trailing edge. Nevertheless, a major step in the theory has now been taken.

In reality, the Reynolds numbers for laminar flow are not high enough for triple-deck theory to be quantitatively accurate. Consequently for practical calculations the interacting boundary-layer theory is more appropriate. This theory was first thought to be merely an approximate model of the flow processes, but it is now known that it is exact in the limit of infinite Reynolds number in the same sense as is triple-deck theory (Burggraf, et al, Ref. 26). The main source of error in the triple-deck appears to be the treatment of the upstream boundary conditions. Because of its asymptotic nature, the longitudinal length scale approaches zero, and hence, the upstream boundary condition (matching to the boundary layer) is applied infinitely far upstream on the triple-deck scale. In contrast, in the interacting boundary-layer model, the upstream condition is that the boundary layer originate at the leading edge. The simplification in the triple-deck case is that Reynolds number can be scaled out of the problem, whereas it must be specified as a parameter in interacting boundary-layer theory. This complication is more than made up for by the improvement in accuracy for practical applications. Experience with the interacting boundary-layer theory indicates that accurate results can be obtained for flows that include regions of separation having moderate transverse extent. The model is likely to fail when breakaway occurs, with its resultant catastrophic reduction of lift. Thus even if breakdown of the theory occurs, it would be an indication of maximum lift conditions.

The computations described above were based either on a time-marching or similar procedure (Rizzetta et al, Ref. 13) or an inverse method of solution (Jobe and Burggraf, Ref. 10; Veldman and Van de Vooren, Ref. 11; Chow and Melnik, Ref. 12). With the latter method, the potential-flow problem is solved for the shape of the displacement surface for specified pressure distribution, and conversely for the boundary-layer problem. (The direct method of solution is unstable.) Both of these methods are slow, requiring severe under-relaxation or small time step to converge; thus long computer runs are required to achieve the steady-state solution. Recently Veldman (Ref. 14) has presented an alternative method, which appears to be significantly faster than either of the above methods. In his method, the potential flow and boundary layer are coupled on a given vertical line and solved together, station by station. Upstream influence is accomplished by iteration on the whole flowfield solution. The method was shown to work well for both unseparated wake flows and for separated flow over contoured surfaces. Consequently, it would appear to be a good method for separated flow past finite airfoils. As will be seen, however, the efficiency of the method deteriorates when the combination of flow separation and wakes occurs.

FORMULATION

Viscous-Interaction Condition

The inverse method invokes viscous interaction by a back-and-forth iterative transfer of information between the potential flow and boundary-layer codes. In contrast, Veldman's (Ref. 14) idea was to compute the boundary layer and potential flow simultaneously station-by-station so that the two flows fully interact at all stages of the iteration process. In Veldman's work, the potential flow was represented by the Hilbert integral of linearized theory, relating pressure to the slope of the displacement surface. This formulation is strictly valid only for small perturbations of the displacement surface from a true plane. However, the idea is readily adapted to a potential flow computation procedure like that of Carlson.

According to linearized theory, the interaction law can be expressed in terms of a Hilbert integral as

$$u_e = u_\infty + \frac{1}{\pi}\int_{-\infty}^{\infty} \frac{v_e\,(\bar{x})\,d\bar{x}}{x - \bar{x}}$$

where (u_e, v_e) are the (x,y) components of velocity at the edge of the boundary layer. In terms of the surface ordinate y_s and the displacement thickness of the boundary layer

$$v_e(x) = u_\infty \frac{d}{dx}(y_s + \delta^*)$$

The inviscid surface speed u_s results from the above Hilbert integral if δ^* is set equal to zero. Hence the deviation of u_e from u_s is given by

$$u_e = u_s + \frac{u_\infty}{\pi}\int_{-\infty}^{\infty} \frac{d\delta^*}{d\bar{x}}\,\frac{d\bar{x}}{x-\bar{x}} \qquad (1)$$

Thus in (1) u_s can be calculated by any potential-flow method, while the displacement correction due to the boundary layer is the given by the Hilbert integral of linearized theory. In the present study, u_s has been evaluated using the Carlson code. In the discretized version the Hilbert integral is truncated at finite limits, resulting in a Cauchy integral; then, using the trapezoidal integration rule, the integral is replaced by a finite sum. Denoting values at the i-th grid point along the x-axis by the subscript i, we have

$$u_{e_i} = u_{s_i} + \frac{u_\infty}{\pi} \sum_{j=0}^{M} c_{ij} \delta_j^* \qquad (2)$$

Veldman gives the values of the c_{ij} corresponding to a uniform grid; we have generalized his derivation to allow for a non-uniform grid, as presented in Appendix A.

In Eq. (2) neither u_{e_i} nor δ_i^* are known a priori, but are related by the solution of the boundary-layer equations, which are solved sequentially at successive stations. Thus at a given station x_i, the values of δ_i^*, for $j < i$ are known (at least in the current approximation) while those for $j > i$ are known only in the preceding approximation. For the values at $j = i$, Eq. (2) is used in the form

$$u_{e_i} - \frac{u_\infty}{\pi} c_{ii} \delta_i^* = u_{s_i} + \frac{u_\infty}{\pi} \sum_{\substack{j=0 \\ j \neq i}}^{M} c_{ij} \delta_j^* \qquad (3)$$

together with the no-slip condition at the surface

$$u = v = 0 \text{ at } y = y_s$$

The boundary-layer equations and the above interaction condition are solved iteratively by marching from x_o to x_M in each iterate

with the unknown terms for $j \neq i$ on the right side of Eq. (2) evaluated from the known solution for the previous iterate. In our application of Eq. (3), a relaxation factor r_v was introduced to allow more flexibility with the calculation; letting the superscript denote the iteration number, we have

$$u_{e_i}^{(n)}/u_\infty - \frac{r_v}{\pi} c_{ii} \delta_i^{*(n)} = u_{s_i}/u_\infty + \frac{1}{\pi} \sum_{j=0}^{M} c_{ij} \delta^{*(n-1)} - \frac{r_v}{\pi} c_{ii} \delta_i^{*(n-1)} \qquad (4)$$

Thus $r_v \to 0$ produces the direct problem, with Goldstein singularity at separation, $r_v = 1$ corresponds to Veldman's approach, and $r_v \to \infty$ yields the inverse problem. Usually the value $r_v = 1$ is satisfactory, but for the higher values of Reynolds number r_v in the range 1.5 to 2.0 is necessary for convergence. Above a certain value of Reynolds number the iteration procedure would not converge for any value of r_v.

Boundary-Layer Formulation

The boundary-layer equations are expressed in terms of Görtler variables in order to reduce the variation of boundary-layer thickness in computational space. Thus the new coordinates s and η are introduced as

$$s = x/c \ , \ \eta = y/\delta$$

where x and y are distances measured along and perpendicular to the airfoil surface (or wake centerline), c is the airfoil chord length, and δ is a thickness scale defined as

$$\delta = [(2\nu c/u_s^2) \int_o^s u_s ds]^{1/2}$$

The non-dimensional stream function $F(s,\eta)$ is introduced, so that the x-component of velocity is given as

$$u = u_s F'(s,\eta)$$

where the prime denotes the η-derivative. The displacement thickness also is given in terms of F, as

$$\delta^* = \int_o^{y_e} (1-u/u_e)dy = \delta(s)[\eta_e - F(s,\eta_e)/F'(s,\eta_e)]$$

The boundary-layer momentum equation then becomes

$$F''' + FF'' + \beta_1 - \beta F'^2 = \beta_2(F' \frac{\partial F'}{\partial s} - \frac{\partial F}{\partial s} F'') \qquad (5)$$

where

$$\beta = \frac{\delta^2}{\nu c} \frac{du_s}{ds}$$

$$\beta_2 = u_s \delta^2 / \nu c$$

$$\beta_1 = (\delta^2/\nu c) \frac{u_e}{u_s} \frac{du_e}{ds}$$

The displacement thickness is rescaled as

$$\Delta^* = \delta^*/\delta = \eta_e - F(s,\eta_e)/F'(s,\eta_e) \qquad (6)$$

Let the subscript i denote the i-th grid point, as $F_i(\eta) = F(s_i,\eta)$. Then in these boundary-layer variables the interaction condition (4) becomes

$$F_i'(\eta_e) - (r_v C_{ii} \delta_i)\Delta_i^* = 1 + \sum_{j=1}^{M} C_{ij}\Delta_j^* - r_v C_{ii}\Delta_i^* \qquad (7)$$

where

$$C_{ij} = (c_{ij}/\pi)(u_\infty/u_{s_i})$$

The interacting boundary-layer problem is defined by Eqs. (5)-(7). In this formulation the Reynolds number R_N occurs only through the variables δ and δ^*, both proportional to $R_N^{-1/2}$.

It may be noted that $u_e = u_s$ for the direct problem, in which case $\beta_1 = \beta$; also in the similarity case F and F' are independent of s so that the right side of Eq. (5) vanishes, and the classical Falkner-Skan equation results. For the interaction problem, u_e (and hence β_1) is unknown and must be determined along with the velocity profile $F_i'(\eta)$.

Numerical Procedure

The computer program is based on a second-order accurate finite-difference representation of Eqs. (5)-(7). The stream function was chosen as primary variable to facilitate treatment of δ^*, as suggested by Eq. (6). Four-point centered differencing is used in the η-variable; typical terms are

$$F'''(\eta_{j-1/2}) = (F_{j+1} - 3F_j + 3F_{j-1} - F_{j-2})/(\Delta\eta)^3$$

$$F''(\eta_{j-1/2}) = (F_{j+1} - F_j - F_{j-1} + F_{j-2})/2(\Delta\eta)^2$$

$$F'(\eta_{j-1/2}) = (F_j - F_{j-1})/\Delta\eta$$

$$F(\eta_{j-1/2}) = (F_j + F_{j-1})/2$$

On the other hand, backward-differencing is used in the s-variable. Either two-point or three-point differencing is available as an option (NX = 2 or NX = 3). For two-point differencing

$$\left(\frac{\partial F}{\partial s}\right)_i = (F_i - F_{i-1})/\Delta s$$

while for three-point differencing

$$\left(\frac{\partial F}{\partial s}_i\right) = (3F_i - 4F_{i-1} + F_{i-2})/2\Delta s$$

For the direct problem, on η=0 the no-slip conditions are $F = F' = 0$, while on the wake centerline $F = F'' = 0$. Also since $u_e = u_s$

$$F' = 1 \quad \text{at} \quad \eta = \eta_e \tag{8}$$

In this case the coefficients of the difference equations form a banded matrix having four non-vanishing diagonals, two of which lie below the principal diagonal. This structure is unchanged by Newton-Raphson iteration and the solution is obtained by a variant

of the Thomas algorithm, described below.

For the interaction problem, the edge condition (8) is replaced by condition (7), which can be written as

$$F_N' + K\Delta^* = R \tag{9}$$

Eliminating Δ^* by use of (6) gives

$$(F_N')^2 + K(\eta_N F_N' - F_N) = RF_N'$$

Since $F_e'' = 0$ we can discretize F_N' as $(F_N - F_{N-1})/h$. Thus the $(N+1)^{st}$ equation is

$$A_{N+1}F_{N-1} + B_{N+1}F_N = 0$$

where

$$A_{N+1} = F_{N-1} - F_N - h(K\eta_N - R)$$

$$B_{N+1} = -Kh^2 - A_{N+1}$$

Linearizing gives the final form for Newton iteration:

$$A^*_{N+1}\delta F_{N-1} + B^*_{N+1}\delta F_N = R^*_{N+1} \tag{10}$$

where δF_N is the change of F_N from one iteration to the next, and

$$A^*_{N+1} = A_{N+1} - F_N + F_{N-1}$$

$$B^*_{N+1} = B_{N+1} + F_N - F_{N-1}$$

$$R^*_{N+1} = -A_{N+1}F_{N-1} + B_{N+1}F_N$$

The interaction problem introduces an additional unknown, β_1; to permit use of the same programming as for the direct problem, the element F_j for $j \leq N$ refers to the stream function

while the element F_{N+1} refers to β_1. The matrix structure is still banded, but in addition its right-most column is non-zero. Thus, the complete system of equations for the Newton iterates has the structure given by (11) below. [Note that P = 0 for the direct problem, while R_j^* represents the error in the original difference equations.] The subdiagonal elements are eliminated line-by-line, proceding from top to bottom; the system of reduced equations is then solved from bottom to top. Convergence of the Newton iterates is rapid. For a boundary layer on a solid surface, convergence to $|\delta F|_{max} < 10^{-6}$ is achieved in four or five iterations with the direct problem, and perhaps double that number for the interaction problem. On passing into the symmetric wake, the iteration count rose to about 20 or 25, falling slowly to the original four or five farther downstream.

$$
\begin{bmatrix}
D_3^* & S_3^* & 0 & 0 & 0 & 0 & \cdots & 0 & P \\
B_4^* & D_4^* & S_4^* & 0 & 0 & 0 & \cdots & 0 & P \\
A_5^* & B_5^* & D_5^* & S_5^* & 0 & 0 & \cdots & 0 & P \\
0 & A_6^* & B_6^* & D_6^* & S_6^* & 0 & \cdots & 0 & P \\
0 & 0^* & A_7^* & B_7^* & D_7^* & S_7^* & \cdots & 0 & P \\
\vdots & \vdots & \vdots & \vdots & \vdots & \vdots & & \vdots & \vdots \\
0 & 0 & 0 & 0 & 0 & \cdots\ A_N^* & B_N^* & D_N & S_N^* \\
0 & 0 & 0 & 0 & 0 & \cdots\ 0 & A_{N+1}^* & B_{N+1}^* & 0
\end{bmatrix}
\begin{bmatrix} \delta F_3 \\ \delta F_4 \\ \delta F_5 \\ \delta F_6 \\ \delta F_7 \\ \vdots \\ \delta F_N \\ \delta \beta_1 \end{bmatrix}
=
\begin{bmatrix} R_3^* \\ R_4^* \\ R_5^* \\ R_6^* \\ R_7^* \\ \vdots \\ R_N^* \\ R_{N+1}^* \end{bmatrix}
\qquad (11)
$$

For the symmetric wake, the system of equations (11) actually begins with an equation for δF_2, the equation for δF_3 also contains the element B_3^*, and that for δF_4 contains A_4^* as well. For the solid wall (located at $\eta_1 = 0$, i = 1,5), the no-slip condition gives $F_1 = F_2 = 0$ so that the first unknown is F_3, as indicated in (11).

For the symmetric wake, F" vanishes instead of F', so that F_1 and F_2 are not known explicitly. Hence the differential equation (5) is solved on $\eta = 0$ as well as for $\eta > 0$. Using the four-point differences listed above we have

$$A_2F_0 + B_2F_1 + D_2F_2 + S_2F_3 + P\,\beta_1 = R$$

(Note P = 0 for the direct problem, while R = 0 for the interaction problem). From the symmetry of the wake flow

$$F_0 = -F_3\ ,\ F_1 = -F_2$$

Hence the centerline equation reduces to the form

$$(D_2 - B_2)F_2 + (S_2 - A_2)F_3 + P\beta_1 = R$$

while for the Newton iterates

$$D_2^*\delta F_2 + S_2^*\delta F_3 + P\beta_1 = R_2^*$$

The solution procedure is unchanged.

The solution of the boundary-layer equations for a single streamwise station is carried out in a subroutine. The Hilbert integral (sum) in Eq. (7) is evaluated in the main program, along with mesh control and overall iteration of the boundary-layer sweeps. The mesh thickness in the η-coordinate is varied to account for the exaggerated growth of the boundary-layer thickness when separation occurs. Δ^* was used to control the mesh thickness, according to the equation

$$(N - N_0)\Delta\eta = \Delta^* - \Delta_0^*$$

where the subscript 0 denotes values with which each boundary-layer sweep are initiated at the leading edge (stagnation point). This scheme permits the shear layer to be well separated from the surface and yet retains the resolution in η needed to allow for the strong shear at the dividing streamline. Mesh-thickness control was found to be essential for the success of the method.

Veldman also used a variable thickness grid, although he used a different technique.

Some special features of the program are summarized below:

- Both direct and interaction modes are allowed. The direct mode is used at the leading edge, a mixed mode is used for $0 < x < x_1$, and full interaction is used for $x \geq x_1$.
- The Rehyner/Flügge-Lötz (Ref. 15) technique (FLARE) is used to stabilize reversed-flow computations.
- Newton iteration is used for rapid convergence at each streamwise station.
- A non-uniform grid is allowed in the streamwise direction, with optional subdivision to improve resolution when needed.
- Optional two-point or three-point backward - differencing of the boundary-layer equations is available in the streamwise coordinate.
- Variable mesh thickness in the η - coordinate is included to account for boundary-layer growth when separation occurs.

DISCUSSION OF RESULTS

Test Cases

Two test cases that exhibit airfoil-like features were run as a check on the program: (1) the flat plate with wake at finite Reynolds number, and (2) the Carter-Wornom dent in an infinite plate. Both of these cases were computed by Veldman (Ref. 1), and the flat plate was computed by Werle and Verdon (Ref. 16), using a semi-inverse iteration scheme due to Carter (Ref. 17).

The flat-plate calculations were carried out for a Reynolds number of 10^5 for both uniform and non-uniform grids (x-only), the latter corresponding to Carlson's airfoil grid referred to above. For the uniform grid, the results compared very well with those of Veldman and of Werle and Verdon. With the non-uniform grid, it was necessary to refine the wake grid-point distribution to achieve satisfactory accuracy downstream of the trailing edge. This point will be emphasized later in the airfoil study. Convergence was rapid for this unseparated flow, with successive iterates for δ^* agreeing to five significant figures after ten iterations.

Computations for the Carter-Wornom dent were made for $R_N = 80{,}000$, with good agreement with Veldman's results. In this case, variable grid thickness was necessary for accuracy owing to the extreme variation of boundary-layer thickness at separation. Convergence was slower than for the unseparated flat-plate flow, requiring 43 iterations for convergence of δ^* to five significant figures.

These test cases incorporate singly two difficult features of viscous interaction: flow separation and wakes. These features combine in flow past airfoils, and it will be seen that convergence is much slower when flow reversal occurs in wakes. For comparison, in the results below for the NACA 0012 airfoil at a Reynolds number of 100,000, convergence to four significant figures required 60 iterations.

Airfoil Results

Interacting flow computations were carried out for two symmetric airfoils at zero incidence: the NACA 0012 Airfoil and the NACA 66_3-018 airfoil (see Figure 2). The 0012 section shape is characterized by adverse pressure gradient over most of the chord, whereas the 66_3-018 shape has minimum pressure at 60 percent chord with adverse pressure gradient aft of that point. Hence these two airfoil sections represent a wide range of flow conditions. Computed results are presented in Figures 3-8 for the 0012 airfoil and in Figures 9-11 for the 66_3-018 airfoil. The effects of computational-grid parameters are indicated in Figures 3-5. Of these parameters, the point of initiation of interaction and grid resolution are the two most important.

For the non-interacting boundary layer on the 0012 airfoil, laminar separation occurs at about 60 percent chord; hence interaction must begin ahead of that point. Various locations of the point (x_1) of initiation of full interaction were attempted from $x_1 = 0.19$ to $x_1 = 0.52$. Converged results for these extremes are shown in Figure 3, in terms of the computed δ^* versus chordwise location from leading edge ($x = 0$) to about one chord length beyond the trailing edge ($x/c = 1$). The results for $x_1 > 0.19$ are unsatisfactory since the interacting and non-interacting flow solutions deviate beyond that point. Consequently the remaining results are for $x_1 = 0.19$. This value is satisfactory for both lower and higher values of Reynolds number, since the separation point is farther aft at lower Reynolds number, and the length of interaction is reduced at higher Reynolds numbers.

The effect of grid resolution is shown in Figure 4. As mentioned earlier, Carlson's program was used to generate the non-interacting potential-flow solution, and the interacting flow solution is then computed on the same non-uniform grid. The results shown here correspond to an x-grid size of about three percent chord on the airfoil, but considerably larger in the wake.

The actual wake-grid points for Carlson's grid are indicated by vertical lines in the figures. A fine grid was generated by interpolating points in the wake such that a nearly uniform grid ($\Delta x \simeq 0.03c$) is obtained from leading edge to the wake cut-off position x_2, where the boundary-layer solution is stopped. Figure 4 shows that use of Carlson's grid leads to very large errors in the wake and, owing to upstream interaction, to significant errors on the airfoil as well. Consequently, only fine-grid results are presented in the subsequent figures. Computation time is increased greatly for the fine grid, since the number of points is doubled in each successive grid interval of the original coarse grid aft of the trailing edge. Thus for N points along the wake centerline in the original grid, $2(2^N-1)$ points are used in the fine grid. In particular, N = 5 for the cases shown in Figure 4 ($x_2 = 2.8c$); thus 62 points are distributed along the wake centerline for the fine grid, versus the original five points. In both cases, 33 grid points were distributed along the airfoil.

The effect of wake-cutoff position x_2 (where the boundary-layer solution terminates) is shown in Figure 5, corresponding to two wake lengths of about one and two chord lengths. The shorter wake appears to be sufficiently accurate, especially on the airfoil itself. Shorter values were attempted ($x_2 = 1.4c$), but were not satisfactory since the reversed-flow "bubble" does not close in that distance (for the NACA 0012 airfoil).

Figure 6 compares results of computations using 2-point and 3-point backward differencing for x-derivatives (NX = 2 and 3, respectively). The more accurate 3-point differencing yields somewhat smaller values of δ^* in the separated-flow region. (The separation point is at x/c = 0.69 for NX = 3, 0.67 for NX = 2.) Recall that the approximation of Rehyner and Flügge-Lötz (Ref. 15) is used, leading to some inaccuracy in the reversed-flow region. Since most of the computations were made with NX = 2, and Figure 6 indicates that they are reasonably accurate, the following Reynolds-number comparisons are for NX = 2.

The effect of Reynolds number on the distribution of skin friction is shown in Figure 7. At the lowest Reynolds number, curve A, R_N = 1000, the flow is completely unseparated and the skin-friction has the highest values. As the Reynolds number increases, separation first occurs at the trailing edge, moving forward to about 70 percent chord at R_N = 10,000, curve B. The skin friction then takes its lowest (most negative) value at the trailing edge. At a higher Reynolds number, curve C, R_N = 100,000, the separation point has moved forward to about 35 percent chord, and the skin friction reaches its most negative value at about 40 percent chord, slowly decaying in magnitude toward the trailing edge as the thickness of the reversed-flow region increases on the airfoil. At this Reynolds number, the separation "bubble" does not close in the wake even for x_2 = 2.8. Attempts to carry out computations at a higher Reynolds number (R_N = 130,000) failed to converge. This lack of convergence for large values of R_N is discussed below.

The effect of Reynolds number on the pressure distributions is shown in Figure 8 for the same cases. Viscous effects lower the suction peak at about 12 percent chord for all three cases, and likewise eliminate the stagnation pressure recovery at the trailing edge in all cases (thus producing pressure drag). The effect of flow separation is most pronounced for R_N = 100,000 (curve C), which shows a nearly flat pressure distribution over the whole separated region, at least beyond the point of minimum skin-friction. This result agrees with the classical Helmholz-Kirchhoff free-streamline theory, recently combined with triple-deck theory by F. T. Smith (Ref. 18) for inviscid separated flow behind bluff bodies.

Turning now to the NACA 66_3-018 airfoil section, we expect certain differences in the viscous characteristics to be apparent. First, the airfoil is designed to have a favorable pressure gradient over the forward 60 percent of the chord length, followed by a rather severe rising pressure. Hence, the laminar

separation point should be nearly fixed in position.* Second, the relatively thick section combined with the rearward location of separation should produce a rather thick separation "bubble" that extends rather far into the wake.

A few computations have been carried out for the 66_3-018 airfoil at Reynolds numbers of 10,000 and 40,000. In this case, the inviscid surface velocity distribution was taken from the tables of Abbott and Von Doenhoff (Ref. 19) and supplemented by use of the Hilbert integral for values in the wake. The grid was essentially uniform in the x-direction, with $\Delta x = 0.05c$, but with finer intervals near the leading edge. Full interaction was initiated at 30 percent chord, since separation is delayed to about 60 percent chord on this airfoil. The wake was computed only to one chord length downstream of the trailing edge, although the results indicate that it should be continued farther.

Figure 9 shows the resulting skin-friction distributions. Separation occurs at about 55 percent chord at both Reynolds numbers compared with the 60 percent location deduced from the inviscid pressure distribution. The most negative skin friction values occur at 60 percent chord, followed by a slow decay toward the trailing edge. This trend is like that for the 0012 airfoil at $R_N = 100{,}000$, corresponding to the thicker separated layer.

The corresponding pressure distributions are shown in Figure 10. Their behavior is similar to the $R_N = 100{,}000$ case for the 0012 airfoil, with deviation from the inviscid distribution occurring near the leading edge and with a suction minimum in the separated region. Unlike the 0012 case, the pressure tends to fall (suction rises) as the trailing edge is approached. However, the computed reversed-flow "bubbles" for both cases

---

* Note that at high Reynolds number, the boundary layer is turbulent and does not separate on the 66_3-018 airfoil at zero incidence.

A and B in Figure 10 do not close up to the point at which the wake computations were terminated. Consequently, these results must be viewed with some reservations.

Computations for the 66_3-018 airfoil at Reynolds number of 100,000 were not convergent, corresponding to a similar failure for the 0012 airfoil at a higher Reynolds number. It is thought that this non-convergence may be caused by thinning of the separated shear layer as Reynolds number increases. This hypothesis is illustrated by Figure 11, which presents the boundary-layer velocity profile at the trailing edge for R_N = 40,000, in terms of the boundary-layer coordinate $\eta = y/\delta$ (see above Eq 5). At this Reynolds number, the nearly stagnant reversed-flow layer is about as thick as the shear layer above it. This comparison would be more pronounced at a higher Reynolds number. A velocity profile of this type is highly unstable, so that turbulence would develop under such conditions. Flow visualization studies of the 66_3-018 airfoil by Mueller and Batill (Ref. 20) show laminar flow to the trailing edge at R_N = 40,000, with oscillatory vortical flow immediately downstream, whereas at R_N = 130,000 the entire separated shear layer appeared to be turbulent. At R_N = 400,000 no separation occurred (for zero incidence), probably because the boundary layer became turbulent upstream of the laminar separation point. These comparisons suggest that the breakdown of the present laminar interaction computations coincides with conditions for which laminar flow ceases to exist in the separated shear layer. The conclusion then is that a reliable boundary layer-transition model is needed for extending the computations to moderately higher Reynolds number.

CONCLUSIONS

The computational results show that the present method for solving the laminar interacting boundary-layer equations is most successful at relatively low Reynolds number where the separated-flow region is small. Convergence is progressively more difficult as the Reynolds number is increased, and the method fails to converge at some value of R_N that depends on the airfoil shape. This breakdown of convergence appears to correspond to conditions for which the viscous shear layer is thin and well-separated from the surface. Such shear layers are highly unstable and transition to turbulence would be expected. Hence, it is concluded that the method works best where laminar flow occurs naturally.

Although the present work was restricted to symmetrical flows, airfoils at angle-of attack could be treated by solving the boundary-layer equations (and interaction condition) separately on both sides of the airfoil. Similar computations have been carried out using the triple-deck model (Daniels, Ref. 21, Chow and Melnik Ref. 12, Mansfield, Ref. 22). However, the separated region would become thicker, and the breakdown of convergence would be expected to occur at lower Reynolds number. The remarks above concerning transition to turbulence apply here as well. The method easily extends to turbulent flow by incorporating a turbulence model in the boundary-layer equations as already carried out by Burggraf (Ref. 23). However, at intermediate Reynolds-numbers where transition occurs in the separated shear layer, a transition model would be required. While such models exist, they are not very reliable. Another area of interest is that of leading-edge separation, for which all of the above remarks apply. In addition, the present method would need to be modified to permit full interaction at (or very near to) the leading edge. In that case, the use of the Hilbert integral as interaction condition would no longer be appropriate; direct coupling of the boundary-layer computation with a full potential-flow solver would be recommended.

APPENDIX A

EVALUATION OF HILBERT INTEGRAL ON IRREGULAR GRID

Two discretized formulations of the Hilbert integral have been given by Veldman (Ref. 14), both for uniform grids. For our purposes, it is convenient to allow a non-uniform grid, and so one of his algorithms is generalized here for that situation. Denote the arbitrarily spaced coordinate values by x_j, $j = 0,1,\ldots,N+1$, where $x_0 < x_1 < \ldots < x_{N+1}$. Then the Hilbert integral in Eq. (1) can be replaced by a finite sum J_i with each term centered in the grid intervals, as

$$\int_{x_o}^{x_{n+1}} \frac{d\delta}{dx}\frac{dx}{x_i-x} \approx J_i = \sum_{j=0}^{N} \left[\frac{d\delta}{dx}\right]_{j+1/2} (x_{j+1}-x_j)/(x_i-x_{j+1/2})$$

where $x_{j+1/2} = (x_j+x_{j+1})/2$, and we drop the superscript (*) for convenience. The limits on the integral x_0 and x_{N+1} are assumed to be sufficiently wide that $d\delta/dx$ is negligible beyond those points. Using central differencing

$$\left[\frac{d\delta}{dx}\right]_{j+1/2} = (\delta_{j+1}-\delta_j)/(x_{j+1}-x_j)$$

Hence

$$J_i = \sum_{j=0}^{N} (\delta_{j+1}-\delta_j)/(x_i-x_{j+1/2})$$

The sum in δ_{j+1} can be reindexed and combined with that in δ_j to obtain

$$J_i = -\sum_{j=1}^{N} (A_j/2)(x_{j+1}-x_{j-1})/(x_i-x_{j-1/2})(x_i-x_{j+1/2})$$

$$- A_0/(x_i-x_{1/2}) + A_{N+1}/(x_i - x_{N+1/2})$$

In terms of the c_{ij} notation of Eq. (3.3), we have

$$c_{i0} = -1/(x_i - x_{1/2})$$

$$c_{ij} = -\tfrac{1}{2}(x_{j+1} - x_{j-1})/(x_i - x_{j-1/2})(x_i - x_{j+1/2})$$

$$c_{i,N+1} = 1/(x_i - x_{N+1/2})$$

This formulation of the Hilbert integral is second-order accurate, consistent with the differencing of the boundary-layer equations. Note that the Cauchy principal value of the integral is evaluated accurately by centering the integrand between adjacent grid points. For a uniform grid, this algorithm reduces to Veldman's simpler version.

APPENDIX B
MULTIGRID MODIFICATIONS TO A POTENTIAL-FLOW CODE

The Multigrid Concept*

Suppose we want to solve the following finite-difference analog to some differential equation:

$$\mathcal{L}_h \phi_h = F_h \tag{B-1}$$

(The subscript h signifies a finite-difference representation on a grid with spacing h.) Further, let us assume that we have some approximation $\hat{\phi}_h$ to ϕ_h and let the difference between the two be $\tilde{\phi}_h$, i.e.

$$\phi_h - \hat{\phi}_h = \tilde{\phi}_h \tag{B-2}$$

Then, if $\mathcal{L}_h$ is a linear operator (as it is in our case)

$$\mathcal{L}_h \phi_h = \mathcal{L}_h \hat{\phi}_h + \mathcal{L}_h \tilde{\phi}_h = F_h \tag{B-3}$$

or

$$\mathcal{L}_h \tilde{\phi}_h = F_h - \mathcal{L}_h \hat{\phi}_h = R_h \tag{B-4}$$

The idea of multigrid is to make use of the fact that we can make useful (and inexpensive) approximations to the above equation (B-4) on a coarser grid, say of mesh size 2h. Thus using some relaxation technique, we solve the equation

$$\mathcal{L}_{2h} \tilde{\phi}_{2h} = I_h^{2h} R_h \tag{B-5}$$

where I_h^{2h} is an operator which transfers to each point on the coarse grid the corresponding value of the residual R_h on the fine grid. The solution is obtained more rapidly on the coarse grid than on the fine grid. Once we have obtained the solution of (B-5) (or at least a good approximation to it) on the coarse

---

* Reference 24 is an excellent treatment of this subject for general applications.

grid, we interpolate the correction $\tilde{\phi}_{2h}$ to the finer grid:

$$\tilde{\phi}_h = I_{2h}^h \tilde{\phi}_{2h}$$

where I_{2h}^h is an interpolation operator. Depending upon a number of factors (grid geometry, interpolation order), the interpolated value of $\tilde{\phi}_h$ may or may not satisfy (B-4) closely enough to be used as a correction to $\hat{\phi}_h$. If not, we simply relax (B-4) a few times and then use

$$\hat{\phi}_{h_{new}} = \hat{\phi}_h + \tilde{\phi}_h \qquad \text{(B-6)}$$

to get a better approximation to ϕ_h, which is the solution of the finite-difference equation of interest. In general, the multigrid procedure uses a sequence of grids, rather than only 2 grids. To achieve fast convergence, the multigrid method relies on the fact that standard relaxation techniques converge rapidly during the initial iterations, but exhibit progressively slower convergence at later stages, especially for fine grids. This is because relaxation techniques are efficient at removing high frequency-error components (i.e.,errors with wavelengths on the order of the grid spacing h), but inefficient at removing low frequency-error components (i.e., errors with wavelengths on the order of the overall grid size). The multigrid method circumvents this difficulty by using a series of coarser grids to eliminate the low frequency-error components. In effect, each of the coarse grids acts as a filter which removes error components with corresponding wave lengths. Peaceman and Rachford (Ref. 25) formulated a method for solving Laplace's equation exactly in a finite number of steps, with one spectral component of the error removed in each step. For NxN grids their method requires of order N^3 operations to obtain the exact solution, whereas the multigrid method requires only of order N^2 log N operations to reduce the error to a specified tolerance.

Application to Potential Flow Past Airfoils

Carlson's (Ref. 1) code has been modified to incorporate the multigrid solution procedure. For efficiency, the transonic code was simplified to allow only the incompressible case. The resulting code then solves the difference equation

$$\nabla_h^2 \phi_h = 0$$

subject to

$$\left(\frac{dy}{dx}\right)_s = \left(\frac{v}{u}\right)_s = \left[(\sin\alpha + \phi_{hy})/(\cos\alpha + \phi_{hx})\right]_s$$

where the subscript s denotes the airfoil surface, and the subscripts x and y denote differentiation with respect to x and y, and

$$\phi_h \to \Gamma_h(\theta-\alpha)/2\pi \quad \text{as } x^2 + y^2 \to \infty$$

where $\tan\theta = y/x$ and $\Gamma_h = \phi_h(x,0^+) - \phi_h(x,0^-)$ for $x > x_{TE}$.

Substitution of $\phi_h = \hat{\phi}_h + \tilde{\phi}_h$ into the above equations leads to the following residual equations for $\tilde{\phi}_h$:

$$\nabla_h^2 \tilde{\phi}_h = R_h^{(1)} \qquad \text{(B-7a)}$$

subject to:

$$\left(\frac{dy}{dx}\right)_s (\tilde{\phi}_{h_x})_s - (\tilde{\phi}_{h_y})_s = R_h^{(2)} \qquad \text{(B-7b)}$$

$$\tilde{\phi}_h \to -\tilde{\Gamma}_h(\theta-\alpha)/2\pi \quad \text{as } x^2 + y^2 \to \infty \qquad \text{(B-7c)}$$

where $\tilde{\Gamma}_h = \tilde{\phi}_h(x,0+) - \tilde{\phi}_h(x,0^-)$ for $x > x_{TE}$.

Here the residuals $R_h^{(1)}$ and $R_h^{(2)}$ denote interior and boundary residuals, respectively;

$$R_h^{(1)} = -\nabla^2 \hat{\phi}_h \qquad \text{(B-8a)}$$

$$R_h^{(2)} = \sin\alpha + (\hat{\phi}_{h_y})_s - [\cos\alpha + (\hat{\phi}_{h_x})_s]\left(\frac{dy}{dx}\right)_s \qquad \text{(B-8b)}$$

Coordinate Stretching

The coordinate stretching scheme of Carlson has been preserved in the multigrid routine. Carlson (Ref. 1) shrinks both the x and y directions onto the finite computational plane ξ,η according to

$$x = x_4 + A_2\tan[\pi(\xi + \xi_4)/2] + A_3\tan[\pi(\xi+\xi_4)^3/2] \quad \text{for} |x|>x_4$$

$$x = \xi(a + b\xi^2) \qquad \text{for } |x|<x_4$$

and $$y = A_1 \tan(\pi\eta/2)$$

where A_1, A_2, A_3, a, b, x_4 and ξ_4 are constants. Then, denoting

$$f = \frac{d\xi}{dx} \quad \text{and} \quad g = \frac{d\eta}{dy}$$

equations (B-7a) and (B-7b) can be written as

$$f(f\tilde{\phi}_\xi)_\xi + g(g\tilde{\phi}_\eta)_\eta = R^{(1)} \qquad \text{(B-9a)}$$

$$\left(\frac{dy}{dx}_s\right) (f\tilde{\phi}_\xi)_s - (g\tilde{\phi}_\eta)_s = R^{(2)} \qquad \text{(B-9b)}$$

where the subscript h on $\tilde{\phi}$ and R is understood. In the new coordinate system, the circulation correction $\tilde{\Gamma}$ is determined from:

$$\tilde{\Gamma} = \tilde{\phi}(\xi,0^+) - \tilde{\phi}(\xi,0^-) \quad \text{for } \xi>\xi_{TE} \qquad \text{(B-10)}$$

The residual functions $R^{(1)}$ and $R^{(2)}$ become

$$R^{(1)} = -f(f\hat{\phi}_\xi)_\xi - g(g\hat{\phi}_\eta)_\eta \qquad \text{(B-11a)}$$

$$R^{(2)} = \sin\alpha + (g\hat{\phi}_\eta)_s - [\cos\alpha + (f\hat{\phi}_\xi)_s] \left(\frac{dy}{dx}\right)_s \qquad \text{(B-11b)}$$

Finite Differences - Governing Equations

Employing second order-accurate differences in ξ and η, equation (B-9a) can be written as

$$[g_j g_{j-1/2}/(\Delta\eta)^2]\tilde{\phi}^+_{ij-1} - [(f_{i+1/2} + f_{i-1/2})f_i/\omega(\Delta\xi)^2 + (g_{j+1/2}+g_{j-1/2})\cdot$$
$$\cdot g_j/(\Delta\eta)^2]\tilde{\phi}^+_{ij} + [g_j g_{j-1/2}/(\Delta\eta)^2]\tilde{\phi}^+_{i,j+1} = R^{(1)}_{ij}$$
$$-[f_i/(\Delta\xi)^2][f_{i+1/2}\tilde{\phi}_{i+1,j} - (f_{i+1/2} + f_{i-1/2})(1-1/\omega)\tilde{\phi}_{ij}$$
$$+ f_{i-1/2}\,\tilde{\phi}_{i-1,j} \qquad \text{(B-12)}$$

where as in Carlson (Ref. 1), ω is a relaxation factor and + denotes new values. The above represents a tridiagonal system of equations for the values of $\tilde{\phi}^+_{ij}$, on a given column, i. Equation (B-12) is solved on columns, sweeping from upstream to down stream.

The residual function $R^{(1)}$ must also be replaced by its finite-difference form. Using second order-accurate differences in ξ and η, equation (B-11a) is represented as:

$$R^{(1)}_{ij} = -[f_i/(\Delta\xi)^2][f_{i+1/2}\hat{\phi}_{i+1,j} - (f_{i+1/2} + f_{i-1/2})\hat{\phi}_{i,j}$$
$$+ f_{i-1/2}\hat{\phi}_{i-1,j}] - [g_j/(\Delta\eta)^2][g_{j+1/2}\,\hat{\phi}_{i,j+1} - g_{j-1/2}\cdot$$
$$\cdot(\hat{\phi}_{i,j} - \hat{\phi}_{i,j-1}) - g_{j+1/2}\hat{\phi}_{i,j}] \qquad \text{(B-13)}$$

Finite Differences - Boundary Conditions

As in Carlson's original program, the residual tangency condition, equation (B-11a) is used to create fictitious values of ϕ inside the airfoil, allowing equation (B-12) to be used as it stands at points immediately outside the airfoil. We expand $(\phi_\eta)_s$ and $(\phi_\xi)_s$ in Taylor series about fictitious points inside the airfoil and replace the resulting derivatives of ϕ by finite differences yielding second-order accurate results.

for the upper surface

$$\tilde{\phi}_{i,jA-1} = 2(\Delta\eta)^2/g_s[3\Delta\eta - 2(\eta_s - \eta_{jA-1})]\cdot$$

$$\cdot\Big\{R_{iu}^{(2)} + g_s[(4\tilde{\phi}_{i,jA} - \tilde{\phi}_{i,jA+1})/2\Delta\eta$$

$$- (\eta_s - \eta_{jA-1})(2\tilde{\phi}_{i,jA} - \tilde{\phi}_{i,jA+1})/(\Delta\eta)^2]$$

$$- (\tfrac{dy}{dx})_s f_s\,[(\tilde{\phi}_{i+1,jA-1} - \tilde{\phi}_{i-1,jA-1})/2\Delta\xi + (\eta_s - \eta_{jA-1})\cdot$$

$$\cdot(\tilde{\phi}_{i+1,jA} - \tilde{\phi}_{i+1,jA-1} - \tilde{\phi}_{i-1,jA} + \tilde{\phi}_{i-1,jA-1})/2\Delta\xi\Delta\eta]\Big\} \qquad \text{(B-14)}$$

and for the lower surface:

$$\tilde{\phi}_{i,jA+1} = -2(\Delta\eta)^2/g_s[3\Delta\eta + 2(\eta_s - \eta_{jA+1})]\Big\{R_{i\ell}^{(2)}$$

$$+ g_s\,[(-4\tilde{\phi}_{i,jA} + \tilde{\phi}_{i,jA-1})/2\Delta\eta - (\eta_s - \eta_{jA+1})(2\tilde{\phi}_{i,jA}$$

$$- \tilde{\phi}_{i,jA-1})/(\Delta\eta)^2] - (\tfrac{dy}{dx})_s f_s[(\tilde{\phi}_{i+1,jA+1} - \tilde{\phi}_{i-1,jA+1})/2\Delta\xi$$

$$+(\eta_s-\eta_{jA+1})(\tilde{\phi}_{i+1,jA+1}-\tilde{\phi}_{i+1,jA}-\tilde{\phi}_{i-1,jA+1}+\tilde{\phi}_{i-1,jA})/2\Delta\xi\Delta\eta]\Big\} \qquad \text{(B-15)}$$

where the index jA denotes the closest point outside the airfoil boundary, and R_{iu} and $R_{i\ell}$ denote residuals for upper and lower surfaces.

Equation (B-14) or (B-15) is first solved on column i using old values from the previous relaxation sweep. Then equations (B-12) are solved for new values exterior to the airfoil along the column i. The new values of $\tilde{\phi}$ so obtained are used in equations (B-14) or (B-15) to generate new values for the fictitious interior points. Thus the interior points are based on new values at station i and old values at other stations as are all points external to the airfoil.

The values of $R_{iu}^{(2)}$ and $R_{i\ell}^{(2)}$ are given in finite difference form by

$$R_{iu}^{(2)} = \sin\alpha - \left(\frac{dy}{dx}\right)_s \cos\alpha + g_s\Big[(-3\hat{\phi}_{i,jA-1} + 4\hat{\phi}_{i,jA} - \hat{\phi}_{i,jA+1})/2\Delta\eta$$

$$+ (\eta_s - \eta_{jA-1})(\hat{\phi}_{i,jA-1} - 2\hat{\phi}_{i,jA} + \hat{\phi}_{i,jA+1})/(\Delta\eta)^2\Big]$$

$$-\left(\frac{dy}{dx}\right)_s f_s\Big[(\hat{\phi}_{i+1,jA-1} - \hat{\phi}_{i-1,jA-1})/2\Delta\xi$$

$$+ (\eta_s - \eta_{jA-1})(\hat{\phi}_{i+1,jA} - \hat{\phi}_{i+1,jA-1} - \hat{\phi}_{i-1,jA} + \hat{\phi}_{i-1,jA-1})/2\Delta\xi\Delta\eta\Big]$$

$$R_{i\ell}^{(2)} = \sin\alpha - \left(\frac{dy}{dx}\right)_s \cos\alpha + g_s\Big[(3\hat{\phi}_{i,jA+1} - 4\hat{\phi}_{i,jA} + \hat{\phi}_{i,jA-1})/2\Delta\eta$$

$$+(\eta_s - \eta_{jA+1})(\hat{\phi}_{i,jA+1} - 2\hat{\phi}_{i,jA} + \hat{\phi}_{i,jA-1})/(\Delta\eta)^2\Big]$$

$$-\left(\frac{dy}{dx}\right)_s f_s\Big[(\hat{\phi}_{i+1,jA+1} - \hat{\phi}_{i-1,jA+1})/2\Delta\xi$$

$$+ (\eta_s - \eta_{jA+1})(\hat{\phi}_{i+1,jA+1} - \hat{\phi}_{i+1,jA} - \hat{\phi}_{i-1,jA+1} + \hat{\phi}_{i-1,jA})/2\Delta\xi\Delta\eta\Big]$$

Computational Procedure and Results

1. Three grid spacings are used: fine, medium and coarse.
2. An initial approximation on the fine grid is obtained by first obtaining an approximation by relaxing on the coarse grid and interpolating these results to the medium grid, where they serve as an initial approximation. Relaxation is again performed on this grid, and these results are interpolated to the fine grid to be used as its starting approximation.
3. The residuals are calculated on the fine grid using (B-8) and are transferred to the coarse grids.
4. A few relaxation sweeps (three are used here) are used on the coarse grid to solve (B-7) (approximately) on that grid.
5. Using quadratic interpolation the coarse grid values of $\tilde{\phi}$ are transferred to the medium grid to serve as an initial approximation to (B-7) there. At the same time, the residuals are transferred to the medium grid.

6. (B-7) is relaxed a few times on the medium grid and the results interpolated to the fine grid. Three relaxations suffice here.
7. In the present problem, it was found necessary to relax three times on the finest grid, after which the new approximation $\hat{\phi}$ to ϕ was found using (B-6).
8. On the fine grid, we relax ϕ three times and check the convergence tolerance: $\max|\Delta\hat{\phi}| < \varepsilon$.

If convergence has not been achieved, new residuals are calculated and Steps 3 to 8 are repeated until convergence to the desired tolerance is achieved. Optimization of the multigrid cycle was not attempted.

Multigrid computations were made at both zero incidence and at an incidence angle of five degrees. In the former case, the method gave the expected improvement in efficiency, but for the latter case there was no significant improvement over the original code. The interior flow computations appeared to behave well, but the circulation about the airfoil converged very slowly. It is possible that an error exists in the program relative to the treatment of circulation on the various subgrids, though a considerable effort to find one was not successful.

To illustrate the method, we take the case of an NACA 0012 airfoil at zero angle of attack. For comparison we list the CPU time on an Amdahl 470 V/6-II computer and the equivalent number of fine-grid iterations used (i.e., iteration on the coarse grid of spacing 2h is 1/4 of an iteration on the fine grid). The same value of relaxation factor was used throughout. The convergence tolerance was set at 10^{-5}.

Finest Grid	No.of Grids	Original Code		Multigrid Code	
		CPU(sec)	Work Units	CPU (sec)	Work Units
25 x 13	2		20	2.2	46
49 x 25	3	19.5	187	5.8	59
97 x 49	3	59.0	114	30.6	71

REFERENCES

1. Carlson, L. A.: Transonic Airfoil Flowfield Analysis using Cartesian Coordinates. NASA CR-2577. 1975.
2. Prandtl, L.: The Mechanics of Viscous Fluids. Division G. Aerodynamic Theory (W. F. Durand, ed.), Vol. 3, pp. 34-208, Springer, Berlin. 1935.
3. Goldstein, S.: On Laminar Boundary Layer Flow Near a Point of Separation. Quart. J. Mech. Appl. Math. 1, pp. 43-69. 1948.
4. Catherall, D., and Mangler, K. W.: Integration of the Two-dimensional Laminar Boundary Layer Equations past the Point of Vanishing Skin Friction. J. Fluid Mech. 26, pp. 163-182. 1966.
5. Crocco, L. and Lees. L.: Mixing Theory for Interaction Between Dissipative Flows and Nearly Isentropic Streams. J. Aero. Sci., Vol. 19, No. 10, pp. 649-679. 1952.
6. Lighthill, M. J.: On Boundary Layers and Upstream Influence. Part II. Supersonic Flows without Separation. Proc. Roy. Soc. London A217, pp. 478-507. 1953.
7. Neiland, V. Ya.: Upstream Propagation of Disturbances in Hypersonic Boundary Layer Interactions. Akad. Nauk SSSR, Izv. Mekh. Zhid. Gaza, No. 4, pp. 44-49. 1970.
8. Stewartson, K., and Williams, P. G.: Self-induced Separation. Proc. Roy. Soc. A312, pp. 181-206. 1969.
9. Messiter, A. F.: Boundary Layer Flow near the Trailing Edge of a Flat Plate. J. Soc. Ind. Appl. Math. 18, pp. 241-257. 1970.
10. Jobe, C. E., and Burggraf, O. R.: Numerical Solution of the Asymptotic Equations of Trailing Edge Flow. Proc. Roy. Soc. London A340, 91-111. 1974.
11. Veldman, A. E. P., and Van de Vooren, A.I.: Drag of a Finite Plate. Proc. 4th Int. Conf. Num. Meth. in Fluid Dyn. Lecture Notes in Physics 35, Springer-Verlag. 1974.

12. Chow, R., and Melnik, R. E.: Numerical Solution of the Triple Deck Equations for Laminar Trailing Edge Stall. Proc. 5th Int. Conf. on Num. Methods in Fluid Dyn. Lecture Notes in Physics 59, Springer-Verlag. 1976.

13. Rizzetta, D. P., Burggraf, O. R., and Jenson, R.: Triple Deck Solutions for Viscous Supersonic and Hypersonic Flow past Corners. J. Fluid Mech. 89, Part 3, pp. 535-552. 1978.

14. Veldman, A. E. P.: Numerical Method for Calculation of Laminar Incompressible Boundary Layers with Strong Viscous-Inviscid Interaction. Report NLR TR 79023, National Aerospace Laboratory, The Netherlands. 1978.

15. Reyhner, T. A., and Flugge-Lotz, I.: Interaction of a Shock Wave with a Laminar Boundary Layer. Int. J. Nonlinear Mech. 3, pp. 173-199. 1968.

16. Werle, M. J., and Verdon, J. M.: Viscid/Inviscid Interaction Analysis for Symmetric Trailing Edges. Report R79-914493-5, United Technology Research Center, E. Hartford, Conn., Jan. 1980.

17. Carter, J. E.: A New Boundary Layer Inviscid Iteration Technique for Separated Flow. AIAA Paper 79-1450, 4th Computational Fluid Dynamics Conference, Williamsburg, Va. 1979.

18. Smith, F. T.: Laminar Flow of an Incompressible Fluid Past a Bluff Body: The Separation, Reattachment, Eddy Properties and Drag. J. Fluid Mech. 92, pp. 171-205. 1979.

19. Abbottt, I. H., and Von Doenhoff, A. E.: Theory of Wing Sections. Dover, New York. 1959.

20. Mueller, T. J., and Batill, S. M.: Experimental Studies of Separation on a Two-dimensional Airfoil at Low Reynolds Number. AIAA J., Vol. 20, No. 4, pp. 457-463. 1982.

21. Daniels, P. G.: Numerical and Asymptotic Solutions for the Supersonic Flow Near the Trailing Edge of a Flat Plate at Incidence. J. Fluid Mech. 63, pp. 641-656. 1974.

22. Mansfield, F. A.: Time Marching Method for Laminar Trailing Edge Flows. M.S. Thesis, The Ohio State University, Columbus, Ohio. 1982.

23. Burggraf, O.R.: Comparative Study of Turbulence Models for Boundary Layers and Wakes. ARL TR 74-0031, Aerospace Research Laboratories, Wright-Patterson AFB, May 1974.

24. Brandt, A.: Multi-level Adaptive Solutions to Boundary-Value Problems. Math. Comp. 31, No. 138, pp. 333-389. 1977.

25. Peaceman, D. W., and Rachford, H. H., Jr.: Numerical Solution of Parabolic and Elliptic Differential Equations. J. Soc. Ind. Appl. Math., Vol. 3, pp. 28-41. 1955.

26. Burggraf, O. R., Rizzetta, D. P., Werle, M. J., and Vatsa, V. N.: Effect of Reynolds Number on Laminar Separation of a Supersonic Stream. AIAA J., Vol. 17, No. 4, pp. 336-343. 1979.

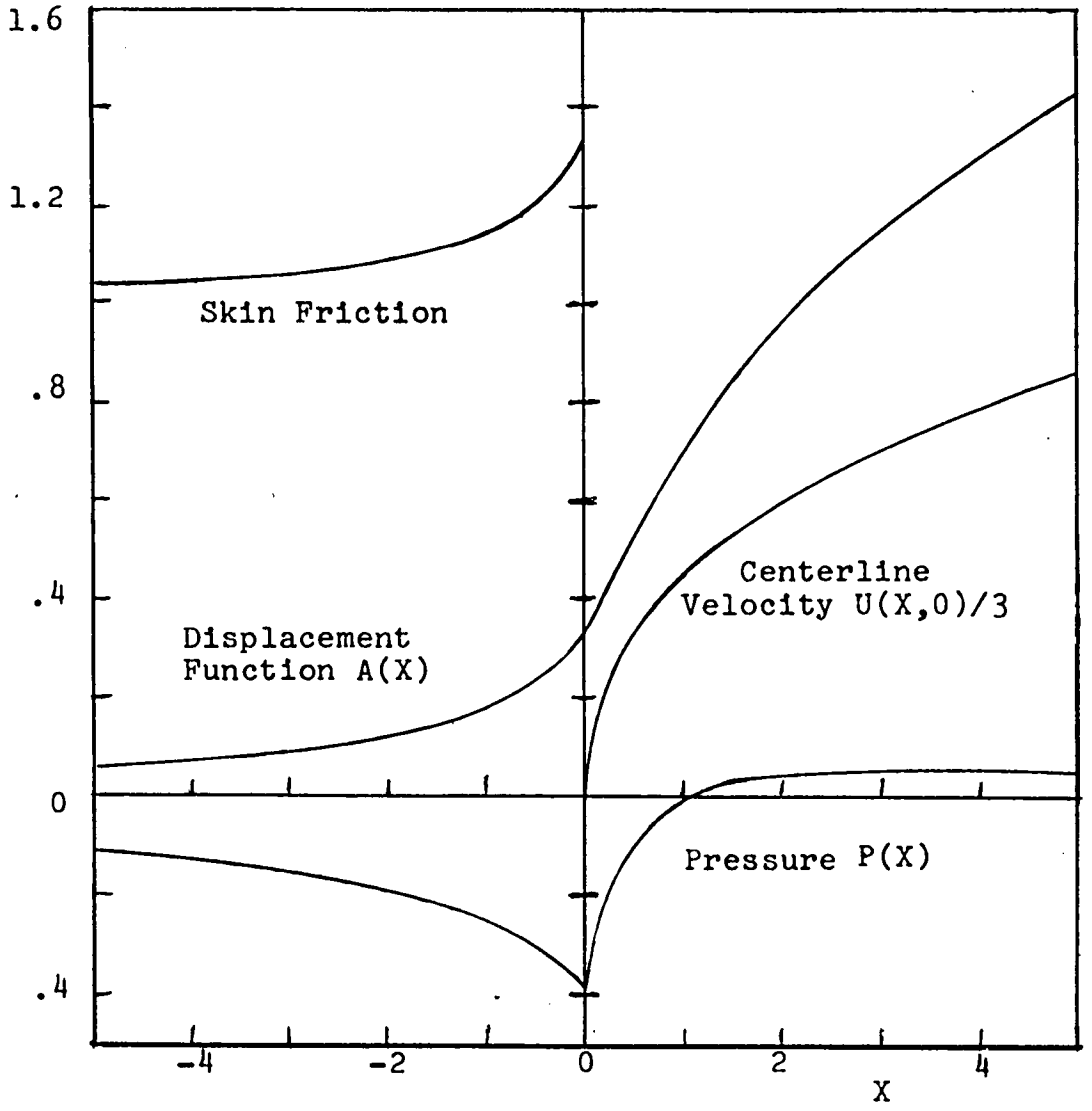

Figure 1. Summary of Triple-Deck Results for Incompressible Trailing-Edge Flow for a Flat Plate at Zero Incidence.

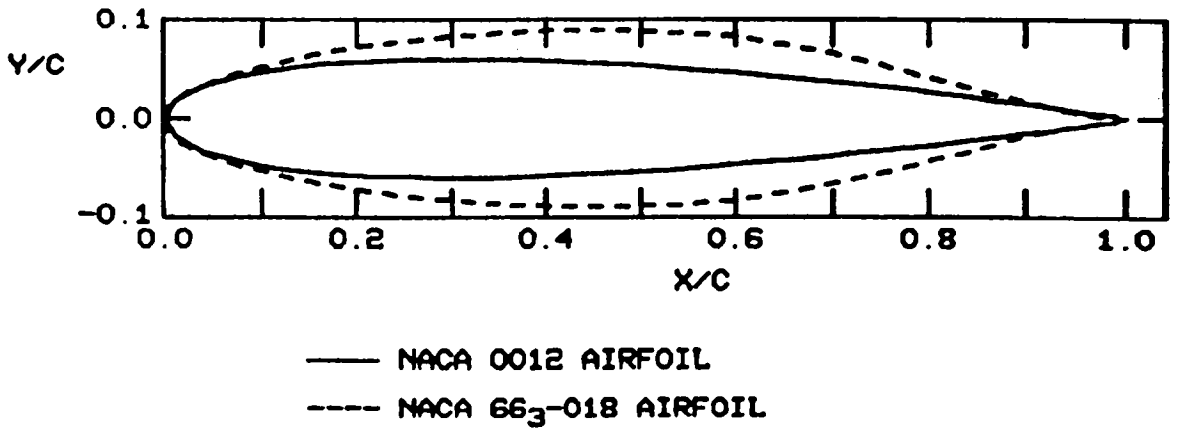

Figure 2. Configuration of Two NACA Airfoils.

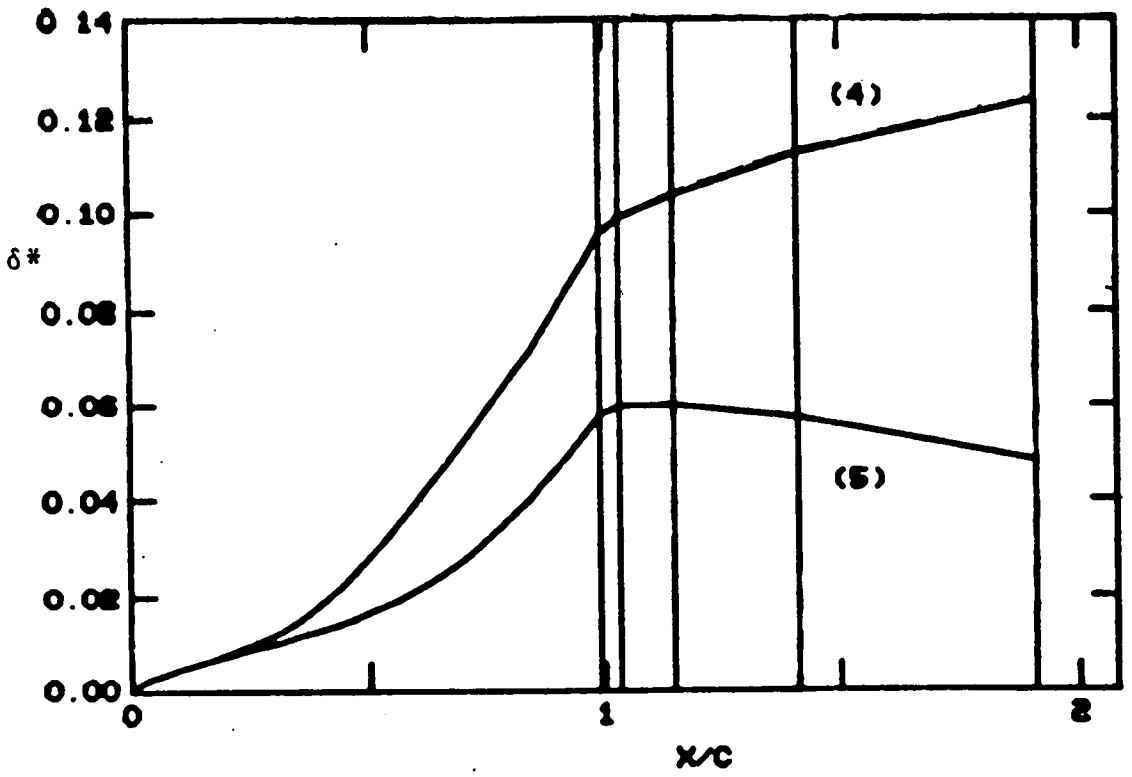

Figure 3. Effect of Point of Initiation of Interaction on Displacement Thickness, for NACA 0012 Airfoil.
R_N = 10,000, NX = 2, Carlson Grid, X_2 = 1.9.
(4) X_1 = 0.52; (5) X_1 = 0.19.

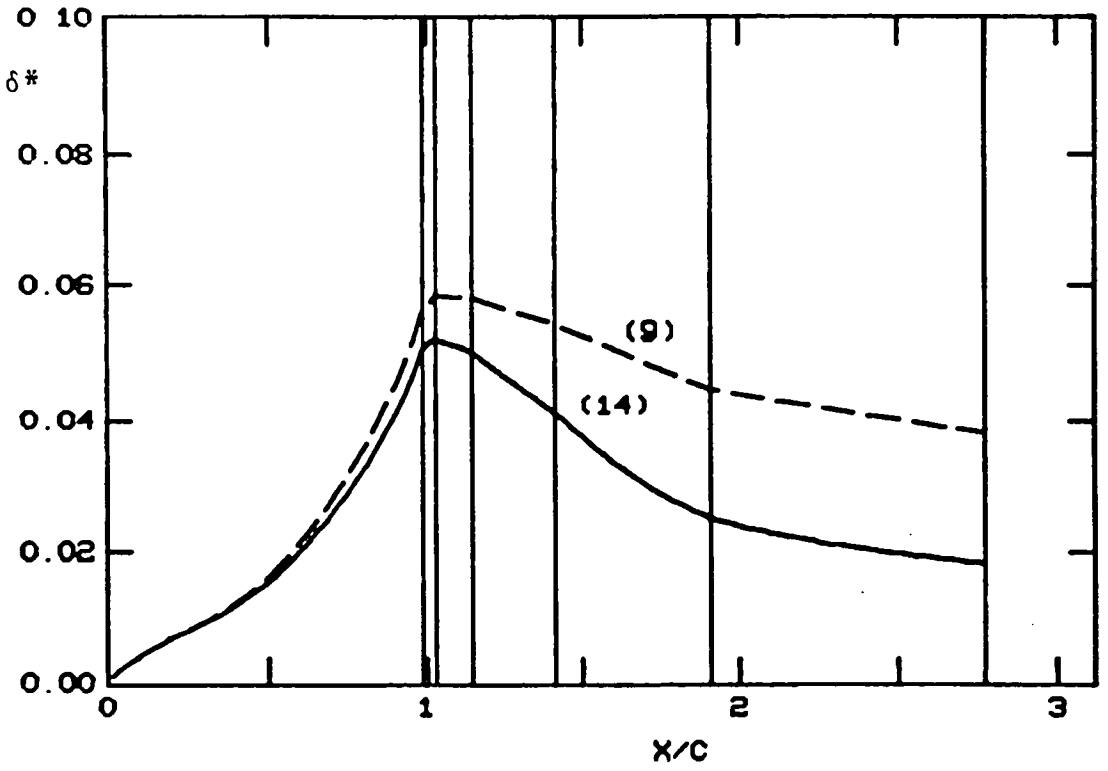

Figure 4. Effect of Grid Distribution on Displacement Thickness for NACA 0012 Airfoil. R_N = 10,000; NX = 2; X_1 = 0.19; X_2 = 2.8. (9) Carlson Grid; (14) Fine Grid.

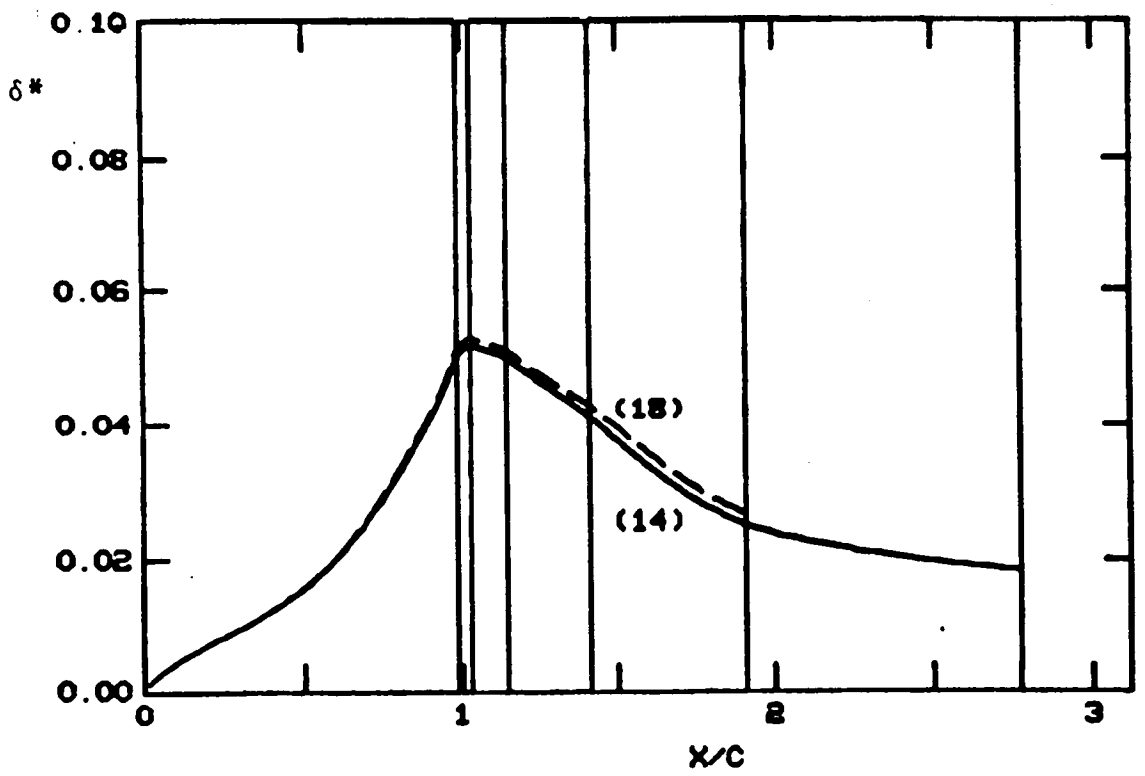

Figure 5. Effect of Downstream Extent of Grid on Displacement Thickness for NACA 0012 Airfoil. R_N = 10,000; NX = 2; Fine-Grid Wake; X_1 = 0.19.
(14) X_2 = 2.8; (18) X_2 = 1.9.

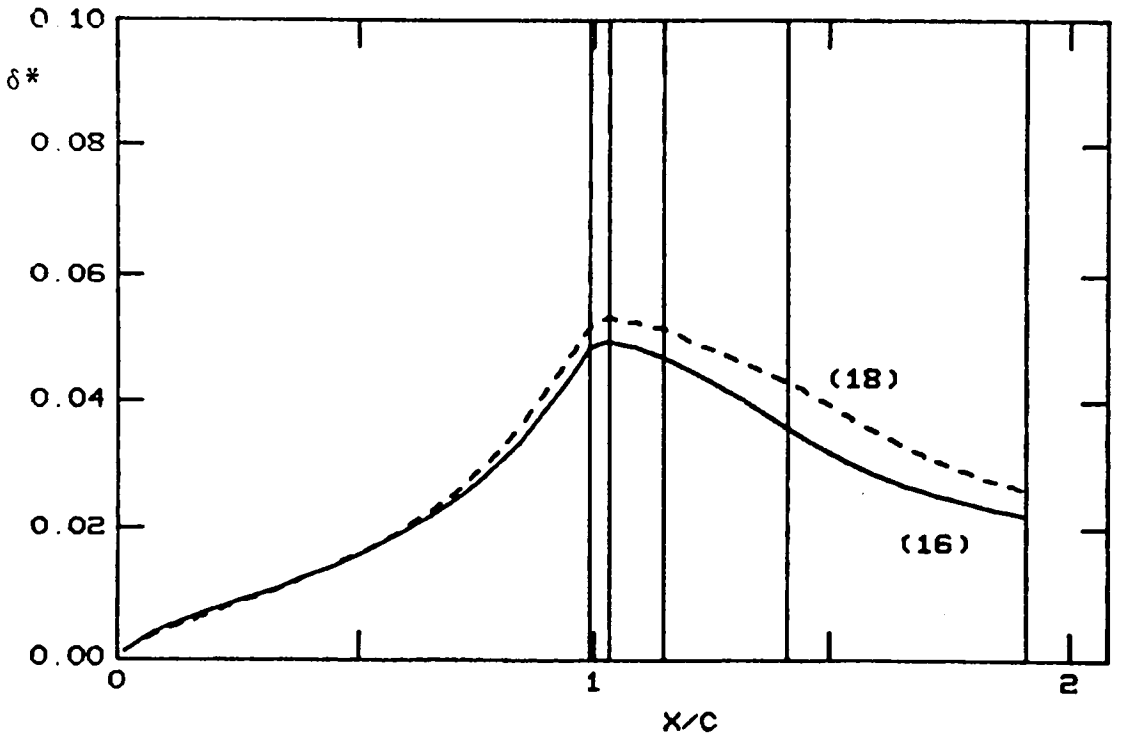

Figure 6. Displacement-Thickness Results for Two-point and Three-Point Integration Schemes for NACA 0012 Airfoil. R_N = 10,000; X_1 = 0.19, X_2 = 1.9. (16) NX = 3; (18) NX = 2.

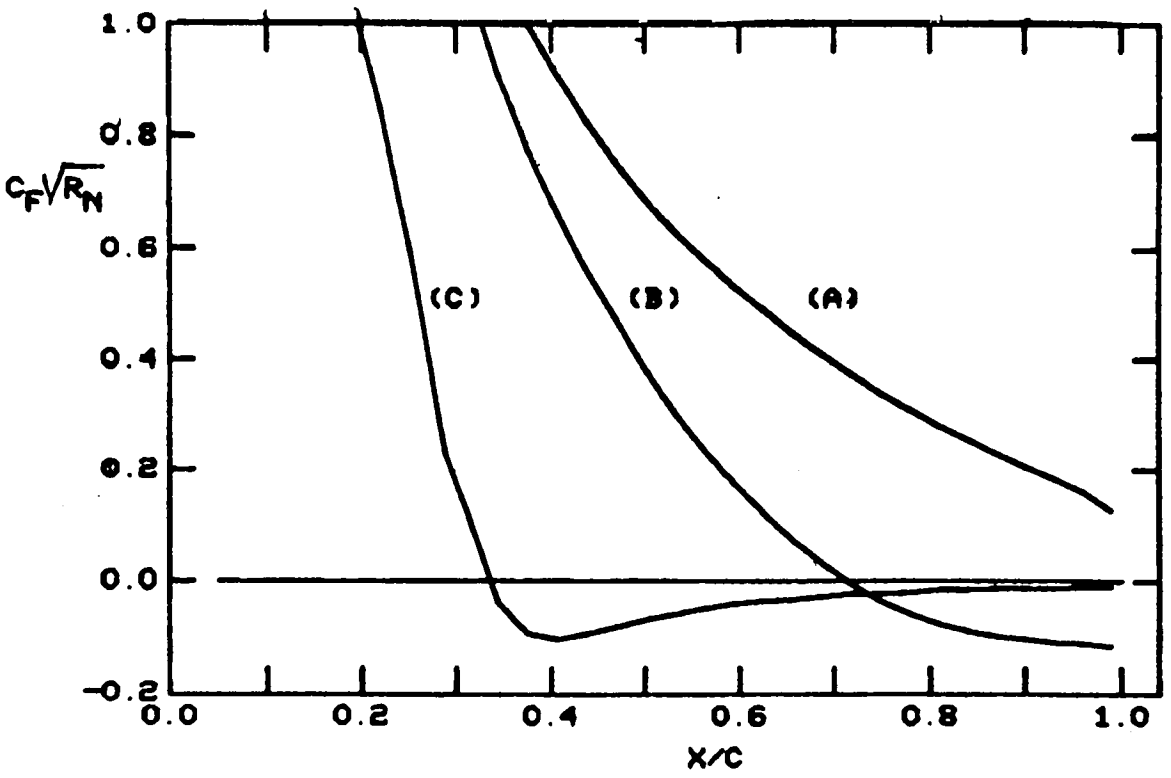

Figure 7. Effect of Reynolds Number on Distribution of Skin-Friction Coefficient for NACA 0012 Airfoil.
NX = 2; Fine-Grid Wake; X_1 = 0.19, X_2 = 2.8
(A) R_N = 1000; (B) R_N = 10,000; (c) R_N = 100,000.

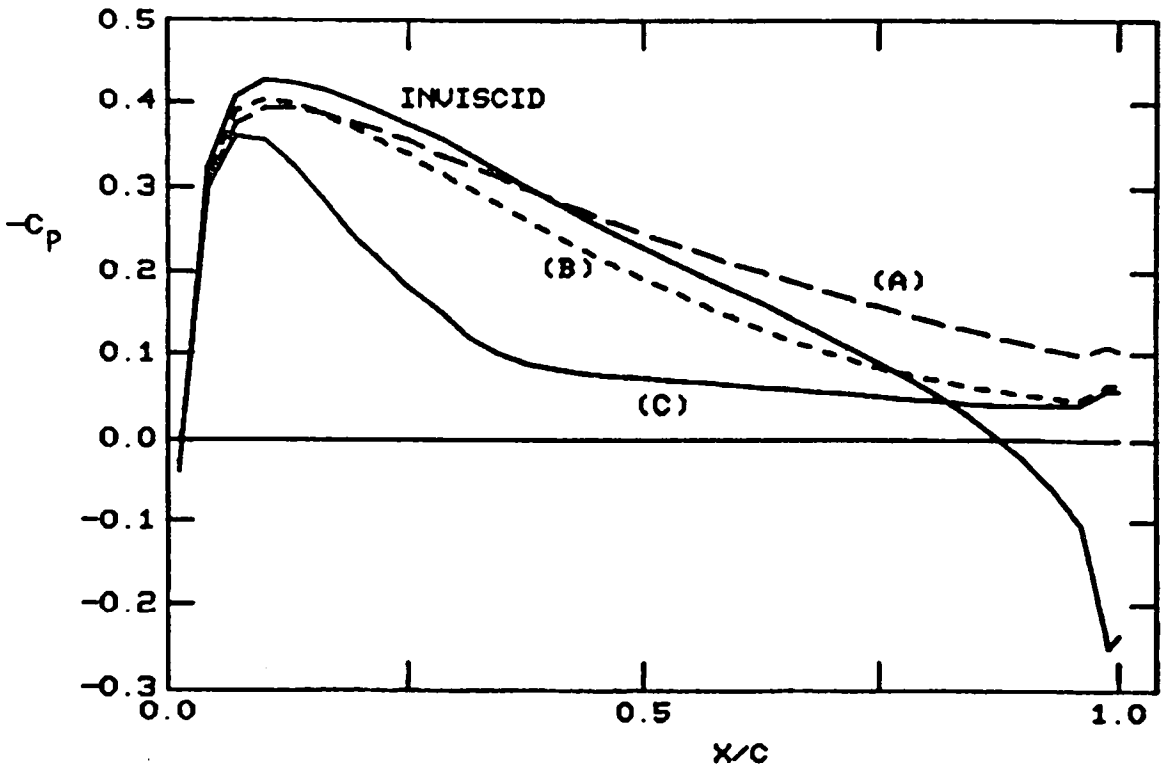

Figure 8. Effect of Reynolds Number on Distribution of Pressure Coefficient for NACA 0012 Airfoil.
NX = 2; Fine-Grid Wake; X_1 = 0.19; X_2 = 2.8.
(A) R_N = 1000, (B) R_N = 10,000; (C) R_N = 100,000.

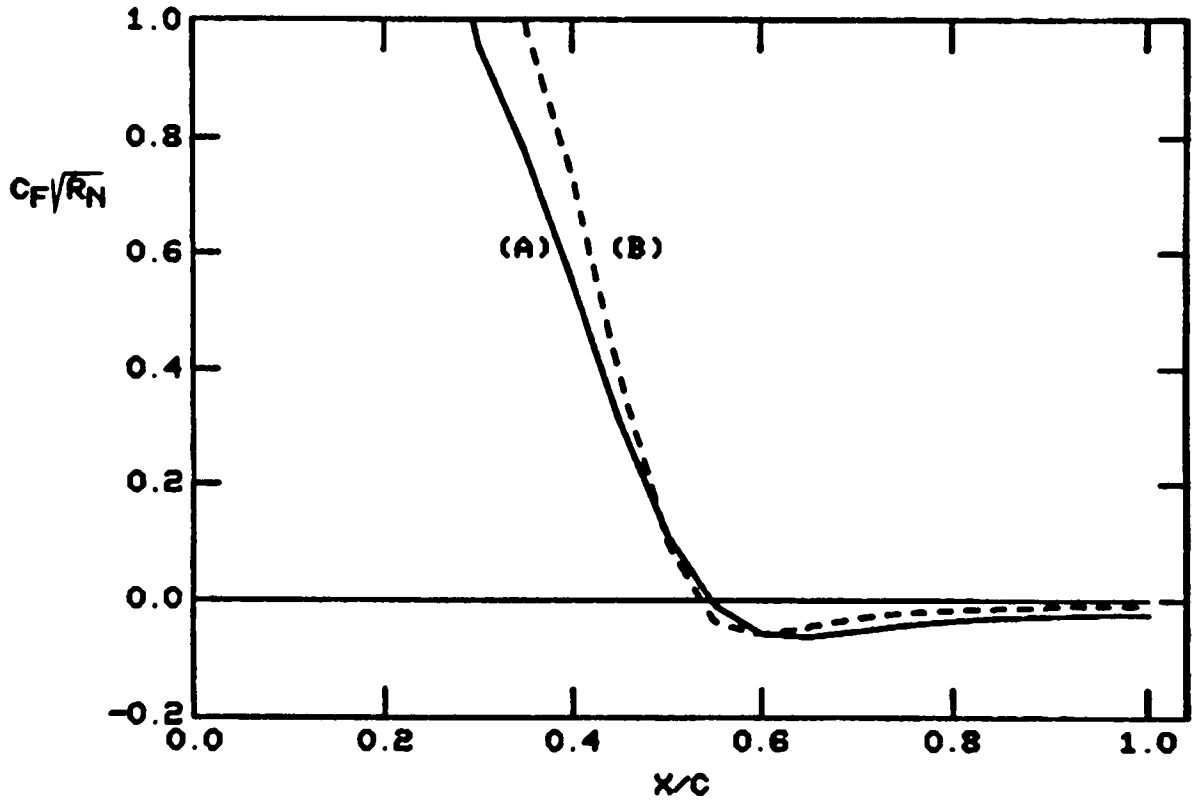

Figure 9. Effect of Reynolds Number on Distribution of Skin-Friction Coefficient for NACA 66_3-018 Airfoil. NX = 2; Fine-Grid Wake; X_1 = 0.30; X_2 = 2.0. (A) R_N = 10,000; (B) R_N = 40,000.

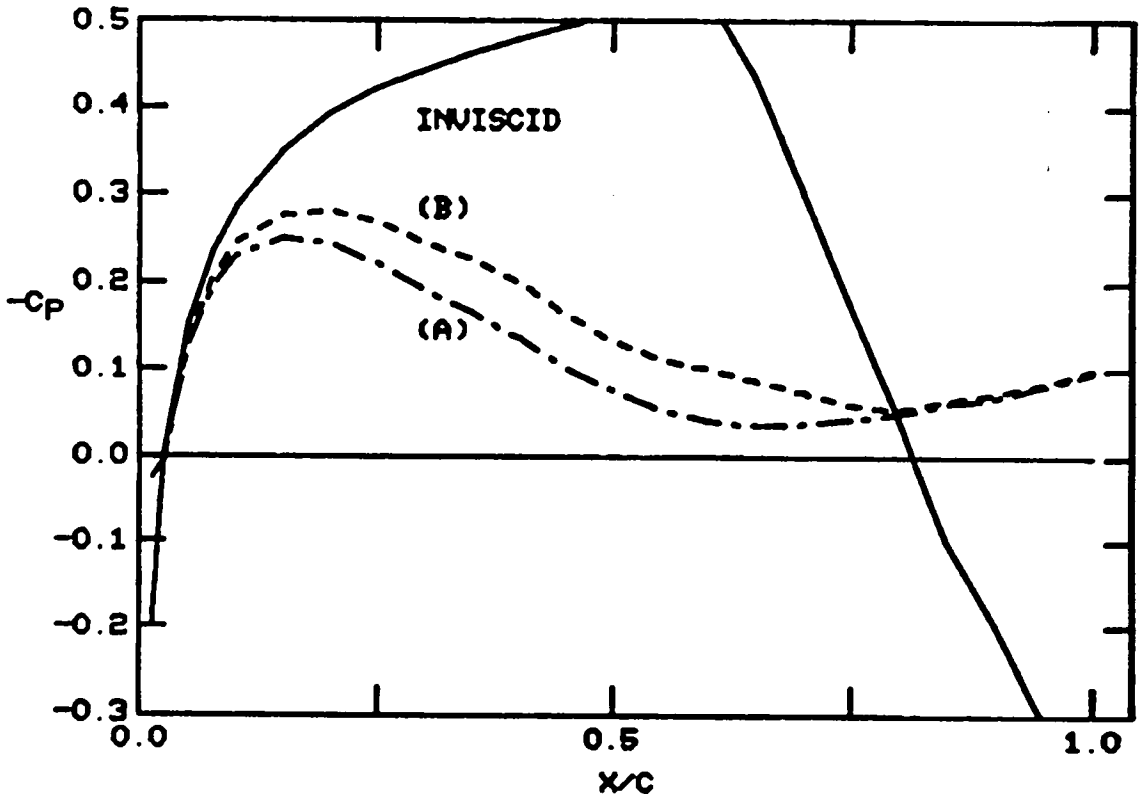

Figure 10. Effect of Reynolds Number on Distribution of Pressure Coefficient for NACA 66_3-018 Airfoil. NX = 2; Fine-Grid Wake; X_1 = 0.30; X_2 = 2.0.
(A) R_N = 10,000; (B) R_N = 40,000.

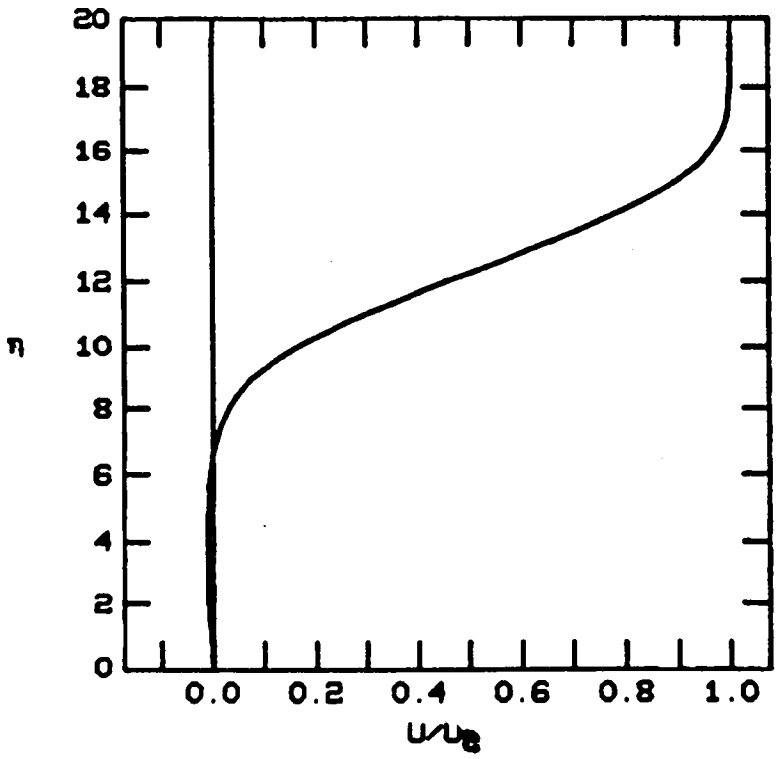

Figure 11. Velocity Profile in Boundary Layer at Trailing Edge of NACA 66_3-018 Airfoil at R_N = 40,000.

1. Report No.	2. Government Accession No.	3. Recipient's Catalog No.
NASA CR-172287		

4. Title and Subtitle	5. Report Date
Interacting Boundary-Layer Solutions for Laminar Separated Flow Past Airfoils	January 1984
	6. Performing Organization Code: 505-31-23-06
7. Author(s): O. R. Burggraf	8. Performing Organization Report No.
9. Performing Organization Name and Address: The Ohio State University Research Foundation, 1314 Kinnear Road, Columbus, OH 43212	10. Work Unit No.
	11. Contract or Grant No.: NSG 1622
12. Sponsoring Agency Name and Address: National Aeronautics and Space Administration, Washington, DC 20546	13. Type of Report and Period Covered: Final Report 4/1/79-3/31/82, Contractor Report
	14. Sponsoring Agency Code

15. Supplementary Notes
Technical Monitor: Joel L. Everhart, NASA Langley Research Center

16. Abstract Numerical solutions of the interacting laminar boundary-layer equations are presented for two symmetric airfoils at zero incidence: the NACA 0012 and the NACA 66_3-018 airfoils. The potential flow was computed using Carlson's code, and viscous interaction was treated following a Hilbert-integral scheme due to Veldman. Effects of various grid parameters are studied, and pressure and skin-friction distributions are compared at several Reynolds numbers. For the NACA 0012 airfoil, Reynolds number is varied from a value just below separation (R_N = 3000) to a value for which extensive separation occurs (R_N = 100,000). For the 66_3-018 airfoil, results are given at intermediate values (R_N = 10,000 and 40,000). The method fails to converge for greater values of Reynolds number, corresponding to the development of very thin well-separated shear layers where transition to turbulence would occur naturally.

17. Key Words (Suggested by Author(s))
Airfoils
Separated Flow
Laminar Boundary Layers
Viscous Interaction

18. Distribution Statement
Unclassified - Unlimited

Subject Category - 02,34

19. Security Classif. (of this report)	20. Security Classif. (of this page)	21. No. of Pages	22. Price
Unclassified	Unclassified	59	A04

For sale by the National Technical Information Service, Springfield, Virginia 22161